Bulletin of Volcanology (2026) 88:1
https://doi.org/10.1007/s00445-025-01867-4

RESEARCH ARTICLE

Growth of a passive lava lake during the 2020–2021 eruption of Kīlauea volcano, Hawaii

Brett B. Carr[1,2] · Matthew R. Patrick[1] · Hannah R. Dietterich[3] · Michael H. Zoeller[1] · Carolyn E. Parcheta[1,4] · Drew T. Downs[1] · Patricia A. Nadeau[1] · Christopher W. Hamilton[2]

Received: 25 October 2024 / Accepted: 22 August 2025

Abstract

We investigate the growth of a passive lava lake in Halema‘uma‘u crater during the December 2020 to May 2021 eruption of Kīlauea volcano, Hawaii. Fed by vents above their surfaces, the formation of passive lava lakes in topographic lows is an important process in the growth of basaltic volcanoes. We captured visible and thermal images during 17 helicopter overflights and applied structure-from-motion photogrammetry to create digital elevation models and orthomosaics of Halema‘uma‘u. These data products allowed us to track eruptive activity and processes. The bulk time-averaged discharge rate (TADR) in December 2020 initially exceeded 100 m^3 s^{-1} but decreased to < 10 m^3 s^{-1} within seven days. By February 2021, TADR was < 2 m^3 s^{-1} and continued to decrease until the eruption ended in May 2021. A total volume of $40.6 \pm 0.5 \times 10^6$ m^3 of lava filled Halema‘uma‘u to a depth of 225 m. As TADR decreased, the lake progressively developed an immobile, solidified crust, beginning with surfaces farthest from the vent. This immobile surface rose endogenously, whereas exogenous surface rise occurred near the vent. Eruptive activity at a vent ended when the level of the lake surface exceeded that of the vent, which we attribute to the effects of lava sitting above the vent on ascending magma. Regular helicopter overflights, combined with field observations and the extensive monitoring network at Kīlauea, generated an unprecedented density of observations that provide insights into the emplacement of passive lava lakes and how these eruptions wane and end.

Keywords Basaltic volcanism · Eruption rate · Lava lake · Structure-from-motion photogrammetry · Kīlauea volcano

Introduction

Basaltic shield volcanoes display a range of eruptive behavior (Walker 1993). The style and duration of eruptions control how the edifice grows and potential hazards (National Academies of Sciences Engineering, Medicine, 2017). Understanding how different eruptive styles contribute to the growth of shield volcanoes and how eruptions begin and end is important for assessing both the short- and long-term hazards associated with these systems. Here, we describe the first eruption to occur at Kīlauea volcano (Island of Hawai‘i, USA) following the 2018 lower East Rift Zone (LERZ) eruption and summit caldera collapse (Neal et al. 2019). After 35 years of continuous activity followed by 2 years of no eruptive activity, the 2020 eruption initiated a new eruptive phase at Kīlauea characterized by a series of comparatively short-lived summit eruptions (Patrick et al. 2023).

On 20 December 2020, fissures opened on the walls of Halema‘uma‘u crater within Kaluapele (Kīlauea caldera) and lava ponded in the topographic low, forming a passive lava lake (see Sect. 1.1. for definition). The formation of passive lava lakes is an important process in the growth of shield volcanoes, filling collapse craters formed during previous eruptions (Swanson et al. 1972, 1979; Harris 2009). However, there are only a few detailed descriptions of the dynamics of these lakes as they form (e.g., Wright et al. 1968; Richter et al. 1970; Peck and Kinoshita 1976). Most

Editorial responsibility: Editorial responsibility: M. Edmonds

✉ Brett B. Carr
bbcarr@arizona.edu

[1] U.S. Geological Survey, Hawaiian Volcano Observatory, Hilo, HI, USA

[2] Lunar and Planetary Laboratory, University of Arizona, Tucson, AZ, USA

[3] U.S. Geological Survey, Alaska Volcano Observatory, Anchorage, AK, USA

[4] Alaska Earthquake Center, University of Alaska at Fairbanks, Fairbanks, AK, USA

previous studies of passive lava lakes described the cooling of ponded lava following the end of an eruption (e.g., Wright et al. 1976; Wright and Okamura 1977; Helz and Thornber 1987; Stovall et al. 2009a) or examined the sequence of layered lavas from an older passive lake exposed in the walls of a newer crater (e.g., Harris 2009).

During the December 2020 to May 2021 eruption of Kīlauea, continuous monitoring from in situ stations and frequent field observations by the U.S. Geological Survey's Hawaiian Volcano Observatory (HVO) collected the most temporally dense set of observations to capture the formation and growth of a passive lava lake. This observational record spans the eruption from start to finish and provides insight into the processes controlling the progression and end of the eruption. Frequent topographic surveys of the lava lake surface as it filled recorded the surface expression of lava flow dynamics within the lake. We present a detailed description of the development of this passive lava lake at Kīlauea to highlight an important process in the growth of basaltic shield volcanoes with implications for the dynamics of ponded lavas and thick, stagnant flows, and the evolution and cessation of eruptions.

Passive lava lakes

Lava lakes can be classified as either active or passive (Swanson et al. 1979; Tilling 1987; Oppenheimer and Yirgu 2002; Stovall et al. 2009a; Lev et al. 2019). Active lava lakes represent the top of the magmatic conduit and can persist for years or decades (Swanson et al. 1979; Tilling 1987; Lev et al. 2019). The 2008–2018 Halemaʻumaʻu lava lake at Kīlauea (Patrick et al. 2018; 2021) and recent lava lake activity at Erebus (Ross Island, Antarctica), Erta Ale (Ethiopia), Nyiragongo (Democratic Republic of the Congo), and Villarrica (Chile) volcanoes are examples of active lava lakes (Lev et al. 2019). Passive lava lakes form when lava collects in a topographic low below a vent and slowly cools and eventually solidifies, due to there being no external heat source to sustain it once lava is no longer flowing into it (Stovall et al. 2009a). One mechanism for the formation of passive lava lakes occurs when a vent opens in the wall of a crater and lava flows down and ponds on the crater floor. Examples of this type of eruptive phenomenon at Kīlauea include the Kīlauea Iki eruption of 1959 (Richter et al. 1970), the 1963 eruption in ʻAlae Crater (Peck and Kinoshita 1976), and the 1965 eruption in Makaopuhi Crater (Wright et al. 1968). Passive lava lakes can also form when lava flows into and fills existing pit craters. This process has been described at Masaya volcano in Nicaragua (Harris 2009) and at Kīlauea during the Maunaulu eruption (Swanson et al. 1972, 1979; Wright et al. 1976). A detailed description of the passive filling of ʻAlae Crater during the Maunaulu eruption based on field observations revealed a complex, episodic sequence of filling and draining that eventually erased any trace of the crater (Swanson et al. 1972).

Eruptions forming passive lava lakes have been observed to end or pause when the level of the lake surface surpasses that of an active vent on the crater wall and "drowns" the vent (Wright et al. 1968; Richter et al. 1970; Swanson et al. 1979). Each of the 17 eruptive episodes at Kīlauea Iki ended when the lake surface reached the vent (Richter et al. 1970). Lava was observed draining back into the vent following the end of the eruptions at ʻAlae, Makaopuhi, and Kīlauea Iki Craters (Wright et al. 1968; Richter et al. 1970; Peck and Kinoshita 1976; Stovall et al. 2009a).

Past observations have shown that the appearance of a stable, solidified surface crust on a passive lava lake is controlled by the rate of inflow into the lake relative to its surface area (Wright et al. 1968; Peck and Kinoshita 1976). During the Makaopuhi and ʻAlae Crater fillings, the entire width of each lava lake showed mobile surface flow during periods of higher effusion rates. When the effusion rate was lower relative to the surface area, lake surfaces furthest from the vent would stagnate and develop a crust (Wright et al. 1968; Peck and Kinoshita 1976). Stagnant areas were characterized by crustal foundering, driven by the density contrast between denser crust and less dense mobile lava beneath and overriding the crust, causing the crust to overturn and sink (Stovall et al. 2009b). The surface of a passive lava lake often slopes slightly downward, away from a high point at the inflow source. Surface flow velocity is generally highest at the inflow and decreases away from the source as flow spreads semi-radially across the lake surface. The lake can also become "perched," where levees bounding the mobile, molten surface form inset of the crater wall with cooler, stagnant, solidified crust at a lower elevation between the levee and wall (Wright et al. 1968; Richter et al. 1970; Peck and Kinoshita 1976).

At Kīlauea Iki, higher effusion rates caused lava from the vent to overflow onto the existing lake surface crust (exogenous growth), whereas when the effusion rate was lower, lava flowed into the lake beneath the crust, causing the lake surface to slowly rise (endogenous growth) (Richter et al. 1970). Endogenous and exogenous surface rise also occurs at active lava lakes (Orr, 2014; Patrick et al., 2014, 2024), as does crustal foundering (Stovall et al. 2009b; Patrick et al. 2016). Patrick et al. (2016) observed larger crustal plates and foundering at the active 2008–2018 Halemaʻumaʻu lava lake when surface velocities were relatively low and smaller plates, with minimal (or no) foundering, when velocities were higher. Crustal foundering also occurs in lava ponds (generally differentiated from lava lakes by their smaller size and absence of a confining crater) that form associated with the emplacement of lava flows (Patrick and Orr, 2011; Orr et al. 2022). Thus, investigation of the eruptive processes driving observed activity at passive lava lakes can inform

the behavior of lava lakes and ponds in general, and their associated flow fields (e.g., Pedersen et al. 2022).

The 2020–2021 eruption of Kīlauea volcano

Prior to the 2018 LERZ eruption of Kīlauea, eruptive activity had been continuous at the summit in Halemaʻumaʻu since 2008 and at Puʻuʻōʻō in the middle East Rift Zone since 1983 (Wolfe et al., 1987; Patrick et al. 2021). During the 2018 LERZ eruption, the Halemaʻumaʻu lava lake drained. The floor of the summit caldera collapsed ~ 500 m at its deepest point as magma withdrew from the summit reservoir and fed lava flows in the LERZ (Anderson et al. 2019; Neal et al. 2019). The end of the LERZ eruption in September 2018 marked the beginning of the first prolonged period of inactivity at Kīlauea in 35 years. Gravity surveys and deformation monitoring indicated that magma was refilling the shallow summit magma reservoir by early 2019 (Poland et al. 2019). In July 2019, a small water lake formed in the bottom of the crater and reached a depth of ~ 50 m over the next 16 months (Nadeau et al. 2024) (Fig. 1).

A new eruption at the summit of Kīlauea began within Halemaʻumaʻu on 20 December 2020, at approximately 21:30 (all times are reported in Hawaii Standard Time), following weeks of elevated seismicity and inflation. Multiple short fissures (~ 50 m long) opened on the talus slopes that made up the walls of the crater, and lava cascaded down into the water lake at the bottom of the crater. The water lake boiled off in ~ 90 min with no significant explosions (Cahalan et al. 2023) as a passive lava lake formed. Also, in the initial hours of the eruption, a buoyant mass of partially submerged more vesicular material (~ 125 m wide and ~ 200 m long) formed and rose with the lava lake, drifting across the lake's surface via the influence of currents in the lava (Fig. 2a–d). We refer to this feature as an "island." While not technically an island due to its buoyancy, there is a long record at Kīlauea for calling similar features islands (Perret 1913; Jaggar 1947; Richter et al. 1970; Wright and Okamura 1977), and we chose to follow precedent. Activity during the initial 24 h of the eruption soon focused at two main locations: (1) a vent on the north wall of the crater that was the dominant effusion source, and (2) a vent on the west

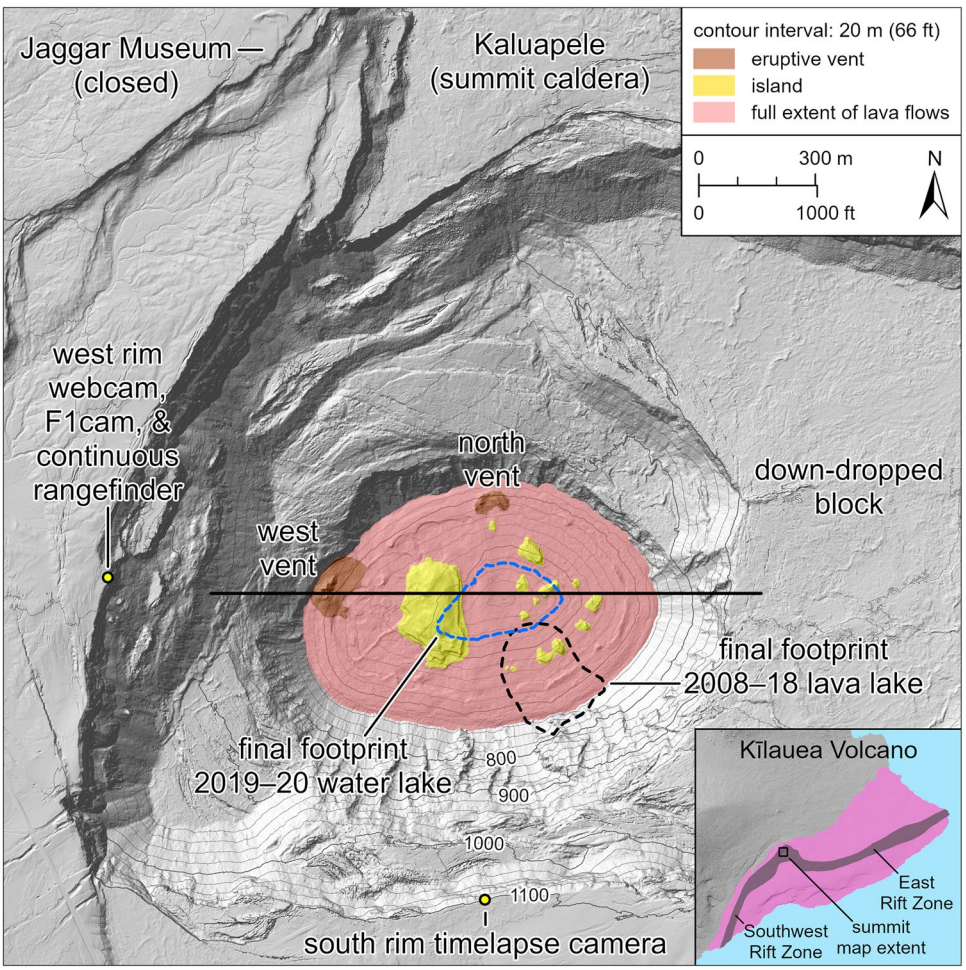

Fig. 1 Halemaʻumaʻu is located within Kaluapele (the summit caldera) at Kīlauea volcano on the Island of Hawaiʻi. Dashed outlines within Halemaʻumaʻu show the extent of the water lake prior to the eruption in December (blue) and the location of the 2008–2018 lava lake (black). Red shading is the final extent of the lava lake from the 2020–2021 eruption, yellow shading shows the islands on the lake surface, and brown shading shows the two main vents. The basemap is a hillshade of a DEM from 2019 (Mosbrucker et al. 2020), except for the lava lake surface, which is the a hillshade from the 8 June 2021 overflight DEM. The horizonal black line is the west to east profile line used for Fig. 4

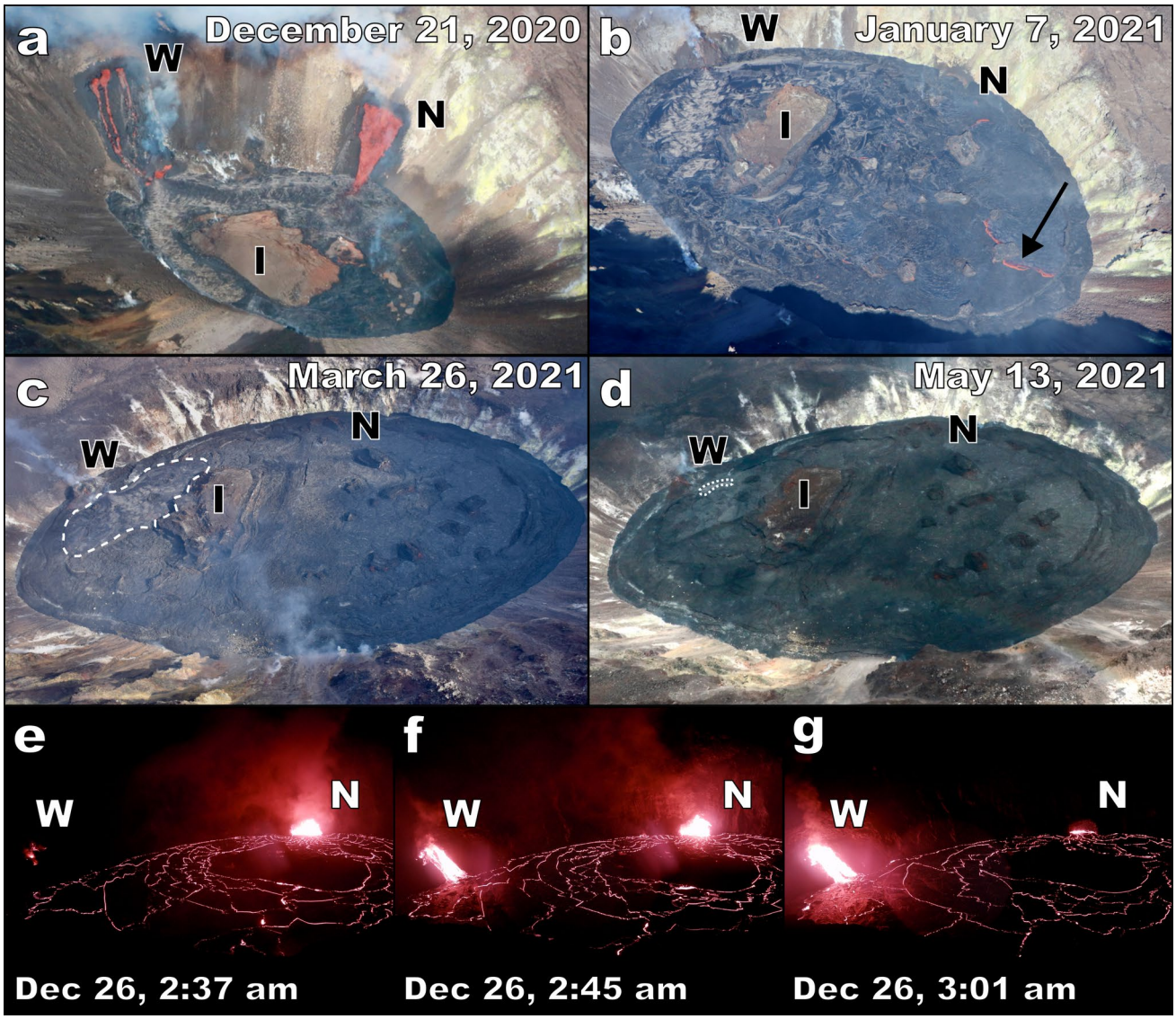

Fig. 2 Photos from helicopter overflights and HVO cameras showed the progression of the 2020–2021 eruption of Kīlauea. **a** On 21 December 2020, erupting lava from both the west (W) and north (N) vents flowed down the crater walls, forming the passive lava lake. The main island (I) is the light brown shape sitting within the lava lake. **b** On 7 January 2021, the north vent was no longer erupting while the west vent remained active. The arrow indicates an active crustal foundering event. **c** The mobile surface area (dotted outline on image from 26 March 2021) was relatively stable in February–April. **d** By 13 May 2021, only a small fraction (dotted outline) of mobile lava surface remained. The look direction of images in a–d is between northwest and north. The W–E (left–right) diameter of the lake is 565 m (**a**), 820 m (**b**), 900 m (**c**), and 910 m (**d**). The shutdown of the north vent on 26 December 2020 was captured by a timelapse camera on the south rim of Halema'uma'u (Fig. 1) showing the north vent as the main active vent with minimal activity at the west vent (**e**), both the north and west vents active (**f**), and the west vent as the main eruptive source with minimal activity at the north vent (**g**). The sequence shown spans 24 min

wall of the crater that was the source of smaller flows and spattering (Fig. 2a).

As the crater filled, the surface of the lava lake surpassed the Level of the north vent on 23 December, and at approximately 03:00 on 26 December 2020, the north vent ceased erupting. A brief period of lava drain back into the north vent was observed and activity at the west vent increased (Fig. 2e–g). The west vent was the only source of effusion for the remainder of the eruption (Fig. 2b–d). The lake surface continued to rise at a progressively slower rate as the diameter of the crater increased with elevation and the effusion rate decreased over time.

During the first week of the eruption (through 25 December 2020), the entire surface of the lava lake was mobile (i.e., the surface had visible incandescence and horizontal flow). After 25 December, the effusion rate decreased and the lake

surface area increased, portions of the lake surface more distant from the erupting vent began to cool and develop a solid, immobile crust. Crustal plates piled up at the lake margins due to surface flow away from the vent, forming a levee and creating a perched lake. As the effusion rate continued to decrease, foundering of crustal plates occurred on the mobile lake surface in areas farthest from the location of lava inflow to the lake. After a period of resurfacing due to foundering lasting hours to days, the crust in the locations where the mobile surface was stagnating would fully solidify and become immobile. We note here that we refer to the portion of the lava lake surface with incandescent and flowing lava as the mobile surface and the portion of the lava lake with a solidified surface crust as the immobile surface. We further note that mobility in this context refers only to the horizonal direction; the immobile surface rose vertically to accommodate the increasing volume of the lava lake (endogenous rise).

The eastern half of the lake surface started to become immobile around 6 January and was completely immobile by 10 January 2021. The immobile surfaces were generally a few meters lower than the mobile lake surface but continued to rise in tandem with the mobile portion as lava flowed into the lake. The surface area of the mobile portion of the lake surface slowly decreased until the eruption ended in late May 2021 (Fig. 1d). No mobile lava was visible on the surface after 23 May, and the last incandescence was observed on 25 May.

Methods

HVO maintains a dense network of monitoring stations around the summit of Kīlauea, which include cameras, seismometers, tiltmeters, and global navigation satellite systems (GNSS) receivers (Shiro et al. 2020). During the 2020–2021 eruption, a Safran Vectronix LRF 7047 laser rangefinder (1550 nm) was set up to continuously measure the rising lava lake surface elevation (Fig. 1) (Younger et al. 2024, 2025). Additional cameras were also deployed to supplement the existing network. HVO staff made field observations and measurements using a Safran Vectronix VECTOR 23 laser rangefinder with hourly-to-weekly frequency while the eruption was ongoing and conducted daily-to-weekly ground-based traverses underneath the eruptive gas plume using a differential optical absorption spectroscopy (DOAS) spectrometer (Ocean Optics SD2000) to measure the emission rate of SO_2 gas (Nadeau et al. 2023). Another key element of HVO's monitoring efforts was frequent helicopter overflights of Halema'uma'u. During these flights, HVO staff collected photographs using a digital single-lens reflex (DSLR) camera and thermal images with a forward looking infrared (FLIR) T1020 camera. In total, 17 overflights were conducted between 21 December 2020 and 8 June 2021. Overflights were initially conducted daily, but the frequency decreased to weekly and then monthly as the eruption progressed and waned (Table 1).

We applied structure-from-motion (SfM) photogrammetry (e.g.Snavely et al. 2008; Westoby et al. 2012; James and Robson 2012) to create 3-D models, point clouds, digital elevation models (DEMs), thermal maps, and orthomosaics using the visible wavelength and thermal images taken during the helicopter overflights. We used Agisoft Metashape Pro v.1.8.1 and followed the workflow of Over et al. (2021) for the SfM processing. Spatial information was added to the models from each overflight using control points identified in photos from two pre-2020 eruption overflights (8 April 2019 and 29 May 2020) and a 2019 lidar DEM (Mosbrucker et al. 2020). We used photos from the pre-2020 eruption overflights to build a pre-eruption model of Halema'uma'u to use as a reference for the topographic differencing discussed below. DEMs and orthomosaics for each overflight were exported at resolutions of 0.5 m and 0.25 m, respectively (Carr et al., 2025).

We applied the M3C2-PM method (Lague et al. 2013; James et al. 2017) within the open-source CloudCompare software (www.cloudcompare.org) to difference the 18 point clouds (the pre-eruption point cloud plus 17 from overflights during the eruption). The M3C2-PM method calculates surface normal distances between two point clouds and a 95% confidence interval for that distance. The confidence interval is determined using the point cloud precision values calculated within Agisoft Metashape Pro following the workflow of James et al. (2020) and the registration error of each cloud to its reference frame (i.e., the pre-eruption model). We restrict the output of the differencing to only the vertical component of the cloud-to-cloud distance to make the result easily transferable to a raster representation of elevation change. For each co-eruptive point cloud, we difference the cloud compared to: (1) the pre-eruption point cloud to calculate the volume of the lava lake, and (2) the point cloud from the previous overflight to calculate the elevation change of the lava lake surface between flights. The cloud-to-cloud vertical distances and their confidence intervals were rasterized at 0.5 m spatial resolution to create maps of elevation change and measurement error.

The lava lake volume and the total measurement error were calculated by summing the pixel values covering the lava lake surface and vents in the elevation change and measurement error maps, then multiplying by pixel area. Thus, reported volumes represent bulk, as opposed to dense rock equivalent (DRE), volumes. This bulk volume represents significantly degassed lava accumulated in the lake between overflights. Drilling of previous passive lava lakes at Kīlauea showed that vesicularity decreased to $< 5\%$ by depths of 15–45 m and density approached DRE values for basalts

Table 1 Eruption parameters for the Halema‘uma‘u lava lake

Overflight Date	Lava Lake Surface Elevation (m) [a]	Maximum Lava Lake Depth (m) [b]	Total Surface Area (m^2) [c]	Mobile Surface Area (m^2) [d]	Volume ($\times 10^6$ m^3) [e]	Volume Error, $\pm(\times 10^6$ m^3)	TADR (m^3 s^{-1}) [f]	TADR Error, $\pm$(m^3 s^{-1})
2020/12/21	628.5	111	164,100	102,000	6.0	0.2	121.2	4.9
2020/12/22	658	140.5	243,300	196,700	11.6	0.4	64.4	6.9
2020/12/23	675.5	158	282,100	245,000	16.0	0.4	52.3	9.4
2020/12/26	695	177.5	332,600	258,900	21.8	0.6	22.9	3.9
2020/12/28	698	180.5	334,400	260,500	22.8	0.8	5.7	7.7
2020/12/30	702.5	185	342,800	255,100	24.4	0.4	9.0	6.8
2021/01/05	708.5	191	364,900	248,000	26.5	0.8	4.2	2.2
2021/01/07	710.5	193	366,400	241,700	27.2	0.5	3.9	7.1
2021/01/12	713.5	196	372,00	141,900	28.4	0.7	2.6	2.8
2021/02/01	726	208.5	408,000	92,900	33.4	0.7	2.9	0.8
2021/02/09	729	211.5	415,200	76,500	34.5	0.6	1.7	1.9
2021/02/16	730.5	213	420,100	68,000	35.3	0.7	1.3	2.3
2021/03/04	734.5	217	427,800	56,800	37.0	0.8	1.2	1.1
2021/03/26	737	219.5	441,400	35,100	38.1	0.4	0.6	0.7
2021/04/16	741	223.5	448,800	32,800	39.8	0.5	1.0	0.5
2021/05/13	742.5	225	448,700	1,800	40.6	0.5	0.3	0.4
2021/06/08	742	224.5	449,000	0	40.3	0.6	–0.1	0.5

[a]Volume-averaged surface. For a given volume, the elevation of the lava lake surface in Halema‘uma‘u if the surface was perfectly flat. Calculated using a pre-eruption digital elevation model (DEM) (Mosbrucker et al. 2020) to the nearest 0.5 m

[b]Maximum depth is calculated as the distance between the volume-averaged surface and the deepest point in Halema‘uma‘u prior to the eruption

[c]Total surface area including both the lava lake and vent areas, rounded to the nearest 10^2

[d]Area does not include islands within the mobile lake perimeter, rounded to the nearest 10^2

[e]Bulk volume (not dense rock equivalent (DRE) volume)

[f]Time-Averaged Discharge Rate (TADR) is calculated over the time between overflights, using bulk volume

(Wright et al. 1976; Helz 1980; Johnson 1979; Mangan and Helz 1986). As the lava lake exceeded 100 m depth on the first day of the eruption, our bulk volumes are likely within 5–10% of the DRE volume, and DRE volume can be estimated by reducing our reported values by that amount. This is a much smaller DRE correction than for bulk volumes for unconfined lava flow fields (e.g., Dietterich et al. 2021), which must be corrected for vesicularity values that range from 20–70%. Although lava vesicularity near the vent and lake surface is certainly higher, we have no samples from which to measure it. The majority of the measurement volume is degassed over the timescales of our observations, so this 5–10% vesicularity correction, which also falls within the measurement uncertainty of the bulk volume, can be reasonably applied over the entire eruption to convert to DRE. We calculated the observed time-averaged discharge rate (TADR) by dividing the difference in erupted (bulk) volume between overflights by the time between flights.

Surface areas (e.g., of the entire lava lake, mobile lava lake surface, and islands) were calculated from polygon shapefiles drawn in QGIS (www.qgis.org) around the perimeter of the features (Carr et al. 2025). Lava lake surface elevation is reported using the “volume-averaged surface level,” which is, for a given volume, the elevation of a flat surface across Halema‘uma‘u containing that volume below it, calculated from the 2019 DEM (Mosbrucker et al. 2020). This avoids local error from measuring elevation at a single point, as was the case for the continuous rangefinder (Fig. 1), which was sensitive to short-term (order of a few hours) fluctuations in the elevation of the mobile surface (Younger et al. 2025). Lake depth is reported as the distance between the volume-averaged surface and the deepest point in Halema‘uma‘u prior to the eruption.

Thermal images from helicopter overflights and a ground-based thermal camera co-located with the continuous rangefinder at Kīlauea’s summit (F1cam, Fig. 1) looking into Halema‘uma‘u (Patrick et al. 2014, 2022) were used to derive multiple data products for the eruption. Thermal maps were created using helicopter overflight images following the thermal data-specific workflow of Patrick et al. (2017) and Carr et al. (2021). Lake surface velocity was calculated following Patrick and Orr (2018) using images from F1cam, with the exception that we used the PIVlab tool in Matlab (Thielicke and Sonntag 2021), not the optical flow toolbox as in Patrick and Orr (2018). This method calculates an array of motion vectors across an image by

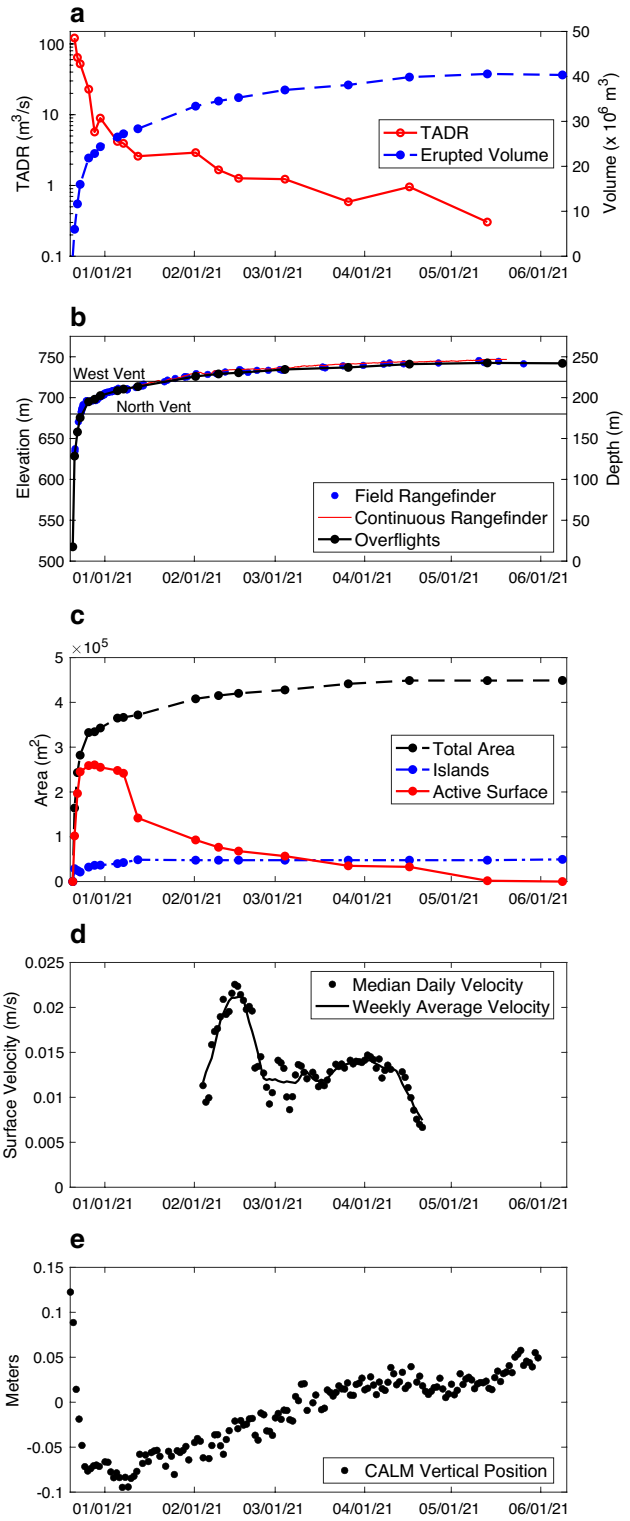

Fig. 3 The bulk TADR (**a**; red, left axis in log scale), bulk erupted volume (**a**; blue, right axis), lava lake surface elevation (**b**; left axis) and depth relative to the lowest pre-eruption elevation (**b**; right axis), total lava lake surface area (**c**; black), mobile lava surface area (**c**; red), island surface area (**c**; blue), lava lake inflow median daily surface velocity (**d**), and GNSS vertical position change (**e**) show the progression of the eruption over its five-month duration. Error for the data in (**a**) is shown in Table 1. Errors for (**b**) and (**c**) are smaller than the symbols representing the data. The low surface velocity values in early February (**d**) are due to a short (2–3 days) stagnation of the mobile surface potentially caused by a reorganization of outflow from the vent and/or a brief decrease in the effusion rate. Data in (**e**) are the daily averaged position from GNSS station "CALM," located on the main down-dropped block from the 2018 collapse in Kaluapele

identifying offsets of features between image pairs (Patrick and Orr 2018). The vector located closest to the location of lava inflow to the lake was used as the inflow velocity. Velocity was calculated every two minutes, but to remove effects of erroneous velocity values caused by atmospheric interference and short timescale (e.g., tens of minutes) flow variations, we use the daily median velocity for our analyses. Data collection for surface velocity was only operational for February–April 2021.

Results

Measurements of TADR, erupted volume, and lake surface rise all show a rapid initial phase of the eruption that decreased as it progressed. In total, $40.6 \pm 0.5 \times 10^6$ m^3 of lava ($38.6 \pm 0.$ 5×10^6 m^3 DRE using 5% vesicularity after Helz 1980) filled Halema'uma'u during the 5-month-long eruption (Table 1; Fig. 3a). The lava lake reached a depth of 225 m with a surface area of 449,000 m^2 at a final elevation of 743 m (all elevations are relative to mean sea level) (Table 1; Figs. 3b–c, 4). More than half of the total volume ($21.8 \pm 0.6 \times 10^6$ m^3 bulk) erupted in the first 5.5 days when the north vent was still active. Due to the inverted cone shape of the crater (Fig. 4), the initial 5.5 days also accounted for over 75% of the lake's depth (177.5 m deep on 26 December, Table 1). TADR exceeded 100 m^3 s^{-1} in the initial 12 h of the eruption but decreased quickly over the following days (Table 1; Fig. 3a). By 30 December (10 days after the eruption began), TADR was < 10 m^3 s^{-1} and by the beginning of February TADR was ~ 2 m^3 s^{-1}. From February through April, TADR was ~ 1 m^3 s^{-1} before decaying in May as the eruption ended.

As the effusion rate decreased, so did the area of the mobile lake surface, in both measured area and relative area as a proportion of the total lake surface, including immobile portions (Fig. 3c). After reaching its maximum surface area on 28 December, the change in the mobile surface area followed trends observed in both TADR (Fig. 3a) and the lake surface velocity near the inflow into the lake (Fig. 3d).

The TADR decreased sharply in January and then stabilized from February through April, before declining to zero as the eruption ended in May. Similarly, velocity was stable in February–April and declined in late April. From 20 December 2020 through March 2021, Halema'uma'u contained the largest known lava lake in the world, temporarily

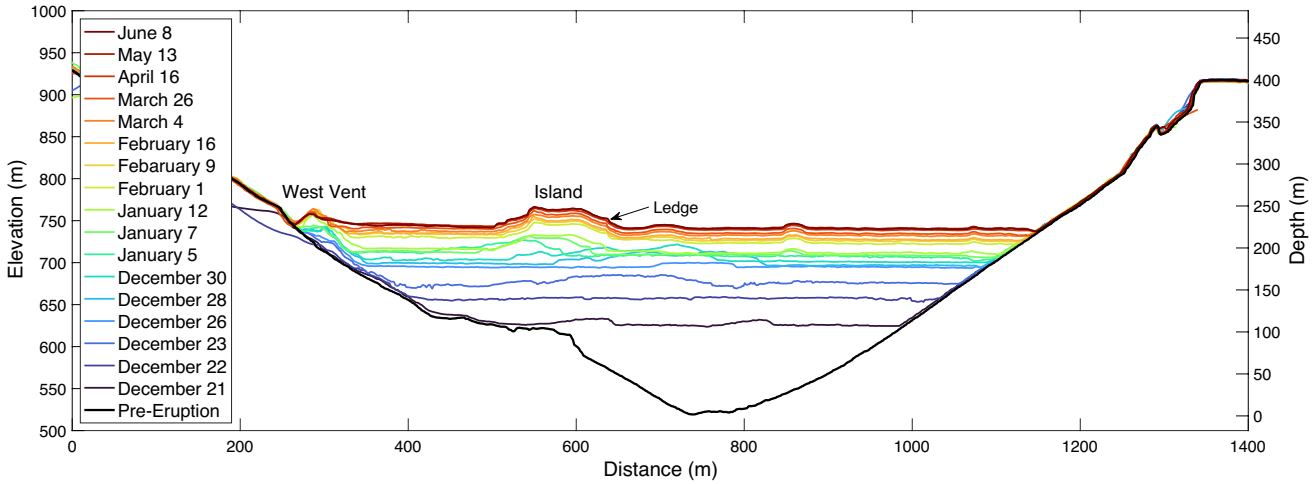

Fig. 4 Topographic profiles from the helicopter overflight derived DEMs across Halema'uma'u show the surface elevation rise (left axis) and increasing depth (right axis) of the lava lake during the eruption. The profile is from west (left) to east (right) and is shown as a black line in Fig. 1

surpassing the surface area of the long-lived active lava lake at Nyiragongo (~ 20,000–50,000 m^2, Burgi et al. 2014; Lev et al. 2019).

Following the short-lived fissure opening phase on the first night, lava erupted from two main vents at 680 m (north vent) and 720 m (west vent) elevation (Fig. 3b). After the lava lake surface reached the elevation of the north vent, the vent cone became attached to the lake surface crust and rose with the immobile surface. The remains of the north vent cone were still visible in the DEM on 13 May (Fig. 5k) at an elevation of 745 m. As the eruption continued at the west vent, the vent cone continued to grow and remained above the lake surface as spatter from fountaining accumulated around the vent. The west vent cone reached a maximum elevation of 762 m on 22 January 2021, more than 40 m above the vent's initial elevation and 20 m above the lake surface elevation on 8 June (Fig. 4).

The rafted "island" of buoyant material initially had a maximum prominence of ~ 15 m above the lake surface and moved (i.e., floated) around the lake (Fig. 5). Following shutdown of the north vent and brief draining of lava into the inactive vent on 26 December, the lake surface dropped, and a ledge of solidified lava ~ 7-m-high formed around the island (Figs. 2, 4, 5). The island's relative buoyancy in the lake remained constant for the rest of the eruption, with the highest point on the island at 22 m above the lake surface (Fig. 4). The island stopped moving horizontally and became "locked" in place by 12 January 2021 (Fig. 5).

The lava lake did not rise evenly across its surface (Fig. 6). The elevation change of the mobile surface (with incandescent flowing lava) often showed a gradient between the vent and margin, generally with greater rise near the vent (Figs. 6a; 6c–d), but also on occasion less rise near the vent (Figs. 6b; 6f), depending on the eruptive activity that occurred between the overflights. Most often, the mobile lava surface rose more relative to the immobile surface between overflights (Figs. 6a; 6 d), promoting the growth of Levees bounding the perched mobile lava surface and a disparity in elevation of 5–10 m between the mobile and immobile surfaces (Fig. 5). However, between 9 February and 4 March, the mobile surface rose less than the immobile surface (Fig. 6b–c). When the mobile surface area stabilized in March–April (Fig. 3c), the mobile surface again rose faster than the immobile surface (Fig. 6d).

The immobile surface rose broadly uniformly. The lake margins (between the perched levees and crater wall) generally showed less rise than the rest of the immobile surface (Fig. 6a–c), except for areas where lava ooze-outs or overflows from the mobile surface were frequent (Fig. 5j), in which case these areas would rise more relative to the interior of the immobile surface (Fig. 6d). Areas where the lake surface elevation decreased were surfaces that had recently transitioned from mobile to immobile (Fig. 6).

Discussion

Passive lava lake dynamics

Growth of the passive lava lake in Halema'uma'u during the 2020–2021 eruption of Kīlauea volcano shared many features with previous passive lava lakes at Makaopuhi Crater, 'Alae Crater, and Kīlauea Iki Crater, but also differed because effusion of lava was continuous, unlike at Kīlauea Iki and Makaopuhi (Wright et al. 1968; Richter et al. 1970), and was sustained for many weeks, unlike at 'Alae

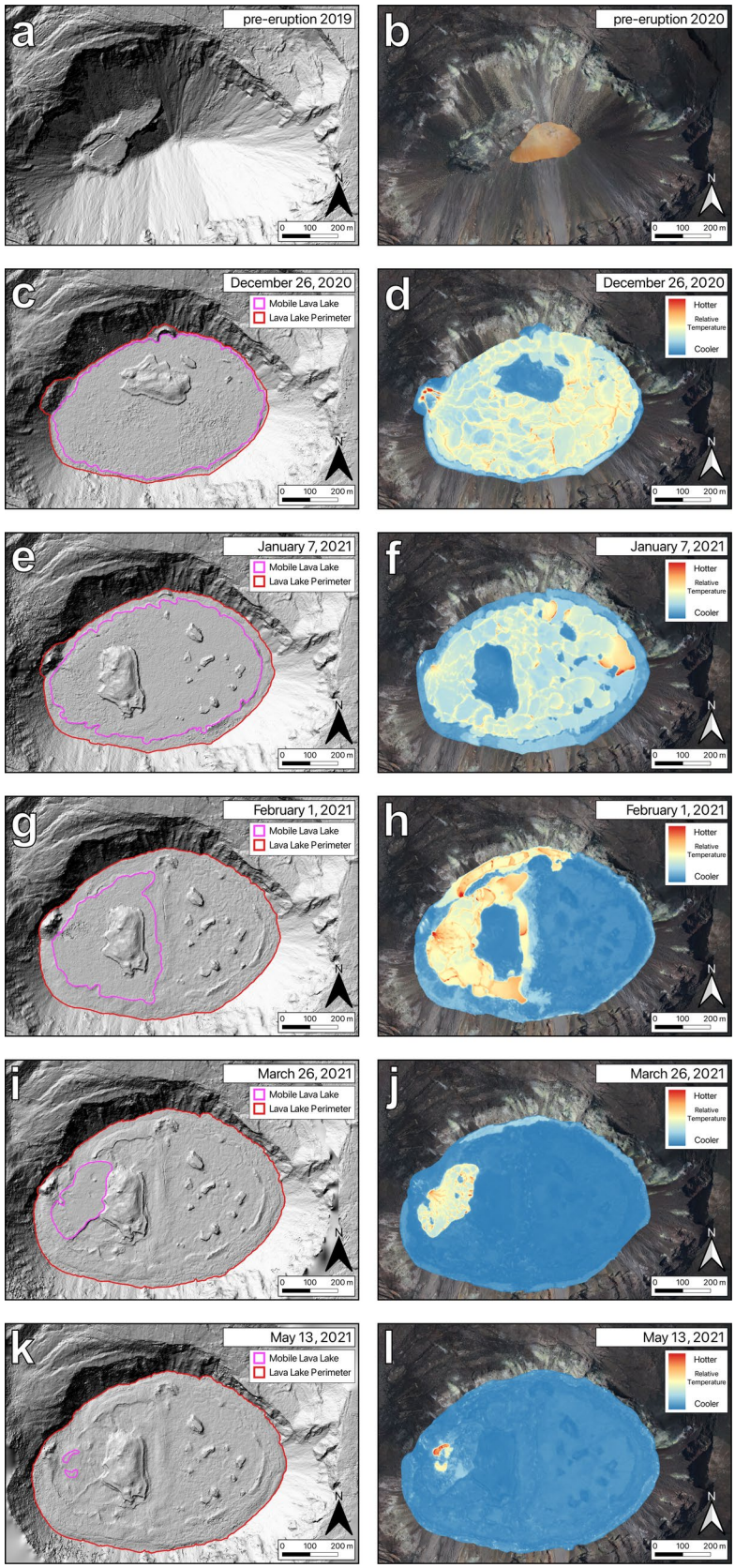

Fig. 5 A selection of five pairs of DEM hillshades (left column) and thermal maps (right column) shows the increasing surface area of the lake (red outline in hillshades) and the decreasing area of the mobile surface (pink outline in hillshades) as the eruption progressed. The pre-eruption hillshade (**a**) is from July 2019 (Mosbrucker et al. 2020). A pre-eruption orthomosaic from a 29 May 2020 overflight is shown in (**b**) and shows the water lake. The colors for thermal maps are relative within each image and do not have the same scale. "Hotter" colors in one image do not indicate that surface temperatures were higher on that day compared to other days. The 7 January 2021 thermal map (**f**) shows an ongoing foundering event on the east half of the lake (hottest part of the surface, also see Fig. 2b). The 1 February 2021 thermal map (**h**) shows an overflow of the mobile lake between the lake levee and the north wall of the crater (red and yellow colors along north edge of the lava lake)

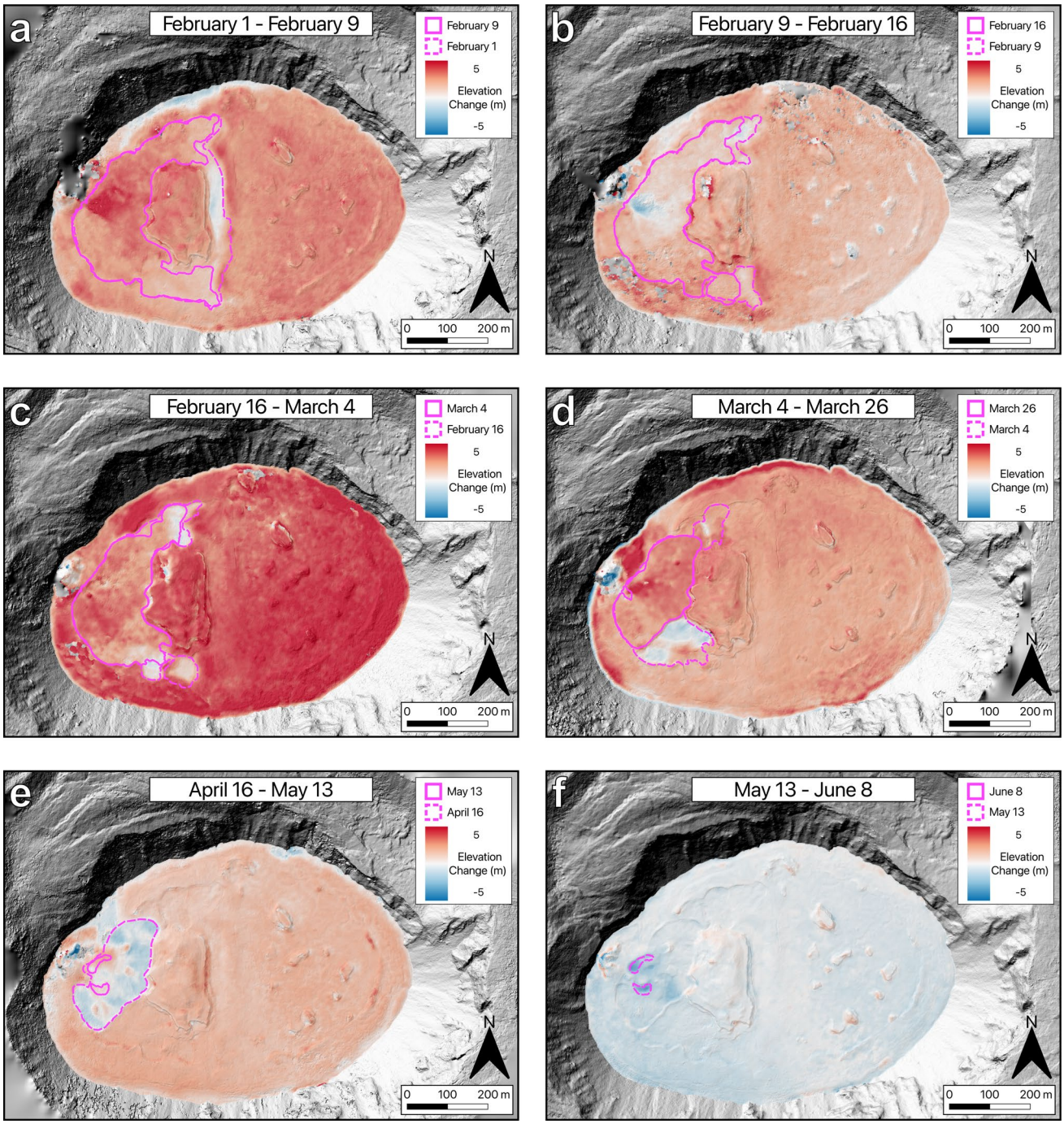

Fig. 6 Elevation difference between DEMs from subsequent overflights shows irregular rise of the lava lake surface. The mobile lava lake surface is marked by pink outlines; the solid line is the perimeter on the newer date, the dashed outline is the perimeter on the older date. The DEM hillshade basemap is from the more recent of the two overflights. The mobile surface (pink outline) generally showed the most rise with higher values near the vent. Newly immobile surfaces (between solid and dashed outlines) show the least rise or surface elevation decrease. The immobile surface (outside both outlines) shows even rise across its surface

and Makaopuhi (Wright et al. 1968; Peck and Kinoshita 1976). During the Kīlauea Iki eruption, onset of new eruptive episodes following pauses were associated with higher effusion rates that led to exogenous emplacement of lava over the existing surface crust (Richter et al. 1970). The Halemaʻumaʻu lava lake in 2020–2021 grew dominantly through endogenous rise, with a mobile surface area around the vents continuously accommodating newly erupted lava. Similar to the ʻAlae, Makaopuhi, and Kīlauea Iki lava lakes, the mobile lake surface in Halemaʻumaʻu sloped downward

by 1–2 m from a high point where lava entered the lake from the vent to the margins. In addition to the vent outflow, this topographic high helped drive horizontal flow of lava away from the vent, a process also observed at the active lava lake in Halemaʻumaʻu during 2008–2018, where upwelling lava was observed creating a positive topographic feature that drove stable flow across the lake surface (Patrick et al. 2016; LeWinter et al. 2021).

The size of the mobile lava lake surface was controlled by the timescale of advection of lava across the mobile surface relative to the timescale of surface crust cooling and thickening. When the crust was sufficiently rigid, it began to buckle and overlap, forming levees that contained the perched mobile lake surface (Fig. 5). Between 26 March and 16 April 2021, when the mobile surface area was constant (Table 1), surface velocity at the lake inflow was also relatively steady at ~ 0.013 m s^{-1} (Fig. 3d). The length of mobile surface flow between the vent and margin Levees was 150–200 m (Fig. 5i–j), which required a travel time of ~ 4 h. Similarly in mid-February 2021, the velocity was ~ 0.022 m s^{-1} and the mobile surface was ~ 300 m from vent to levee, also requiring a travel time of ~ 4 h. Following work by Wilson and Parfitt (1993) for the formation of perched lava ponds, the crust thickness (δ, in meters) can be estimated as $\delta \sim \sqrt{\kappa t}$ and the flow thickness (D, i.e., the thickness in meters of the horizontally flowing lava of the mobile lake surface) as $D = \sqrt{\delta / q^2}$, where $\kappa \approx 10^{-6}$ m^2 s^{-1} is the thermal diffusivity, t (seconds) is the time since the lava was erupted, q is the ratio of crust to flow thickness when motion stops, and $q^2 \approx 1/300$ was found empirically by Hulme and Fielder (1977). For a cooling time of ~ 4 h, this gives a crust thickness of ~ 12 cm and a horizontal flow unit thickness of ~ 6 m. As TADR decreased throughout the 2020–2021 eruption, the horizontal flow velocity also decreased and the mobile surface area receded (Fig. 3), leaving a series of abandoned levees across the solid, immobile surface (Fig. 5). The mobile surface area was a good approximation of relative TADR on a scale of days to weeks (Fig. 3), a relationship that was previously described by Wilson and Parfitt (1993), who suggested that the size of a perched lava pond can be used to approximate the rate of the eruption that formed it.

Elevation changes of the mobile and immobile surfaces of the lava lake provide insight into the movement of lava within the lake. The perched mobile lake surface rose as lava accumulated within the confining levees. The mobile surface area consisted of recently erupted lava flowing horizontally that was vesicle-rich and had lower bulk density compared to the older lava already in the lake. Previous studies of passive lava lakes show a sharp increase in density and decrease in vesicularity from the surface towards the interior over a distance of a few meters (Wright et al. 1976; Peck 1978). Orr et al. (2022) show that for ponds in a perched lava channel, vesicularity can decrease from > 50% at the surface to near-zero at ~ 3 m depth. We propose a model of surface flow similar to that of Orr et al. (2022) and Peck and Kinoshita (1976), with the mobile surface consisting of a relatively thin layer (a few meters compared to the total lake depth of hundreds of meters) of vesicular lava moving horizontally above the relatively stagnant and dense lava below, and a relatively sharp boundary between the two layers (Fig. 7). This two-layer model is supported by our calculation of a relatively thin mobile surface from the velocity-distance timescale (Wilson and Parfitt 1993). Further evidence in support of a thin, mobile surface layer is the observation of islands in the mobile surface that remained stationary as lava flowed around them. These island blocks were rooted in the stagnant deeper layer, a process also observed and described in Orr et al. (2022). As the flowing lava slowed, cooled, and outgassed towards the margins of the mobile surface, its density increased and the lava integrated with the stagnant layer below, likely resulting in downwelling flow in the near subsurface away from the mobile surface margins. A similar mechansim was proposed by Peck and Kinoshita (1976) for the ʻAlae Crater passive lake. Occasionally, lava from the mobile area was also emplaced exogenously onto the immobile surface when the levee broke or was overtopped.

When a section of surface transitioned from mobile to immobile as the mobile area retreated, the lava supply to the area via horizontal surface flow stopped. Once the supply of lava into an area ceased, the surface subsided from the level of the mobile surface to the level of the immobile surface (Fig. 7). This process caused newly immobile surfaces to show the least surface rise or surface elevation loss in overflight data (Fig. 6). When the eruption ended and there was no longer any horizontal flow, a shallow pit formed within the levees that had contained the last zone of the mobile surface (Figs. 5k, 6e–f). The 13 May to 8 June elevation difference, a mostly post-eruptive time span, shows widespread surface subsidence (Fig. 6f), a process also observed at previous passive lava lakes at Kīlauea, which has been attributed to gas loss and thermal contraction (Swanson et al. 1972; Wright et al. 1976; Wright and Okamura 1977; Peck 1978).

The immobile surface, while static horizontally, rose uniformly and endogenously by the continued accumulation of erupted lava beneath the surface crust (Fig. 7). The uniform rise and level surface elevation of the immobile surface suggests that any horizontal lava motion beneath the crust was decoupled from the immobile surface crust above it. The lake margin between the levees and the crater wall was filled by repeated overflows from the mobile surface or ooze-out flows breaking through the levee or crust (Figs. 5h, 7), similar to the seeps observed at perched lava ponds (Patrick and Orr 2012; Orr et al. 2022). As the crust within this area rose endogenously, gaps formed between the crust and

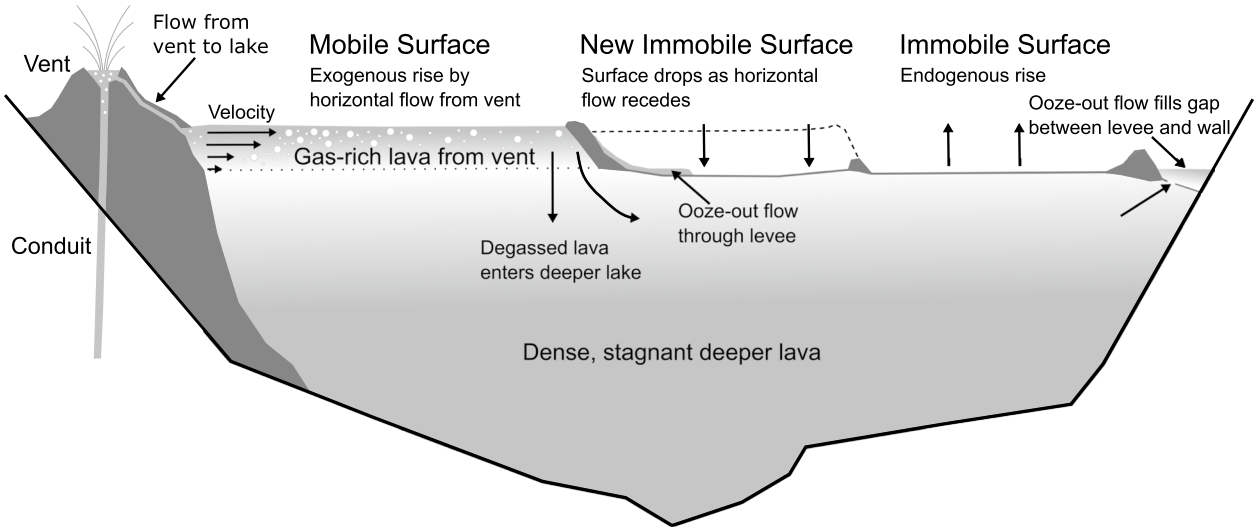

Fig. 7 The mobile surface of the lava lake rises exogenously due to horizontal flow from the vent as a relatively thin and gas-rich layer above the denser, stagnant lava in the deeper lake. Immobile surfaces rise endogenously due to upwelling from below. When a surface transitions from mobile to immobile, the surface drops as the horizontal flow from the vent recedes. The surface in the area between the crater wall and lake levee rises exogenously due to ooze-out flows breaking out from the levee or crust. Overflows and ooze-outs from the mobile surface would also occasionally emplace lava exogenously onto the immobile surface. Figure is not to scale

crater wall creating space for the ooze-outs to emerge and fill in, so the elevation of the surface along the lake margins rose exogenously as well (Figs. 5h, 5j, 6d, 7). The process of ooze-outs filling the space between lava lake levees and crater walls was also observed in passive lava lakes during the Makaopuhi and Kīlauea Iki eruptions (Wright et al. 1968; Richter et al. 1970).

Eruption waning and end

Previous passive lava lake eruptions were observed to pause or end when the lake surface reached the level of the highest vent, with lava often draining back down the vent (Wright et al. 1968; Richter et al. 1970; Peck and Kinoshita 1976). This suggests that lava sitting above the vent can significantly buffer the driving pressure of bubble expansion and escape from the erupting lava, thereby increasing lava density, slowing ascent, and promoting positive feedback mechanisms that decrease the mass flux rate and further slow or completely suppress ascent (Wright et al. 1968; Bruce and Huppert 1989; Wilson et al. 1995; Jones et al. 2017). The north vent in Halema‘uma‘u stopped erupting—though not immediately—after lava exceeded its elevation. Rangefinder measurements of the surface elevation show that lake Level reached that of the north vent up to 2.5 days prior to effusion stopping and that as much as 15 m of lava was above the vent when it stopped (Fig. 3b). A surge in lava effusion was observed at the west vent ~ 15 min prior to activity at the north vent ending, indicating that most of the ascending magma rerouted from the north to the west vent (Fig. 2e–g).

We suggest that the vent switch occurred as increasing lava overburden pressure at the north vent eventually suppressed magma ascent to the north vent, driving it towards the west vent. The feasibility of this hypothesis can be tested with a calculation of the difference in hydrostatic head between the vents. In the near-surface, ascending magma will take the path of least resistance to the surface, so for the higher elevation west vent to be preferred over an inundated but lower elevation north vent, the ratio of the density of the erupting lava to the density of the lava in the lake sitting above the vent must equal the ratio of the depth of lava above the north vent (15 m) to the elevation difference between the north and west vents (40 m), a value of 0.375. If we assume a DRE density of Kīlauea basalt of 2800 kg m^{-3} (from a likely range of 2700–3100 kg m^{-3}; Greenland et al. 1988; Moore 2001; Sutton et al. 2003; Carbone et al. 2013; Dietterich et al. 2021) and vesicularity of 75% for the erupting lava (Sparks 1978; Greenland et al. 1988; Stovall et al. 2009b; Carbone et al. 2013), this yields an erupting lava density of 700 kg m^{-3} and a density of 1867 kg m^{-3} (33% vesicularity) for the near-surface mobile layer of lava in the lake, both reasonable values based on previous studies of erupted lava at Kīlauea (Richter et al 1970; Wright and Okamura 1977; Wolfe et al. 1988; Wilson et al. 1995; Carbone et al. 2013; Orr et al. 2015, 2022; Jones et al. 2017; Dietterich et al. 2021). Thus, it is possible that a sufficient mass of higher density lake lava sitting above the north vent led lower density ascending lava to favor the higher elevation, but unburdened, west vent.

Numerous datasets (e.g., overflight photogrammetry, continuous rangefinder, lake inflow surface velocity, GNSS displacement, SO_2 emissions, earthquake counts) show that the eruption ended in May 2021 following a period of decreasing activity that began in mid-April (Figs. 3; 6; 8). This decaying phase of the eruption corresponded with the lava lake surface elevation exceeding the elevation of effusion from the west vent. It was not possible to directly observe this because outflow from the vent had been crusted over since February. However, in January, flow from the west vent was observed at an elevation of ~ 745 m, measured in the field with a laser rangefinder (Fig. 8a–b). From this observation, we infer the west vent cone developed an insulated conduit stretching ~ 25 m above the initial vent location on the crater wall. The vent cone also reached its maximum elevation in late January, suggesting that increase of the vent outflow elevation also stopped around this time. The continuous laser rangefinder on the rim of Kaluapele (Fig. 1) shows that the mobile lava lake surface reached 744 m elevation in mid-April (Fig. 8c–d). After the lava lake surface reached this elevation, lake surface rise (Fig. 8d) and SO_2 emissions (Fig. 8e; Nadeau et al. 2023) declined, whereas both inflationary deformation (Fig. 8f) and the number of earthquakes at the summit (Fig. 8g) increased from April into May. These signals point towards a decreased rate of lava supply into the lake and increased accumulation of ascending magma in the shallow storage region beneath Halema‘uma‘u without erupting.

Monitoring data support an interpretation that the vent was slowly drowned starting in mid-April and over the following 3–4 weeks (Fig. 8). During this time, the lake continued to rise above the vent outflow elevation, and the effusion rate declined until the eruption stopped in late May, when the mobile surface elevation was 746 m (Fig. 8d). While 2 m of lava above a vent may not seem to be sufficient to suppress magma ascent, the density contrast between the erupting and ponded lava is a key factor (Greenland et al. 1988), and previous works have shown that relatively small ponding depths above vents can have a significant effect on outflow. Wilson et al. (1995) and Jones et al. (2017) demonstrated that < 2 m of ponded lava over a vent can significantly reduce eruption velocity and lava fountain height and that this effect is enhanced for low mass flux eruptions. Magma ascending in a dike also loses more heat as it slows, becoming more viscous and moving even slower, a positive feedback process that can promote eruption stagnation (Bruce and Huppert 1989). As TADR was 0.3 $m^3\ s^{-1}$ between 16 April and 13 May, and 1 $m^3\ s^{-1}$ in the 2.5 months prior (Table 1), it is feasible that even a small amount of lava sitting above the vent was sufficient to further slow ascent (by

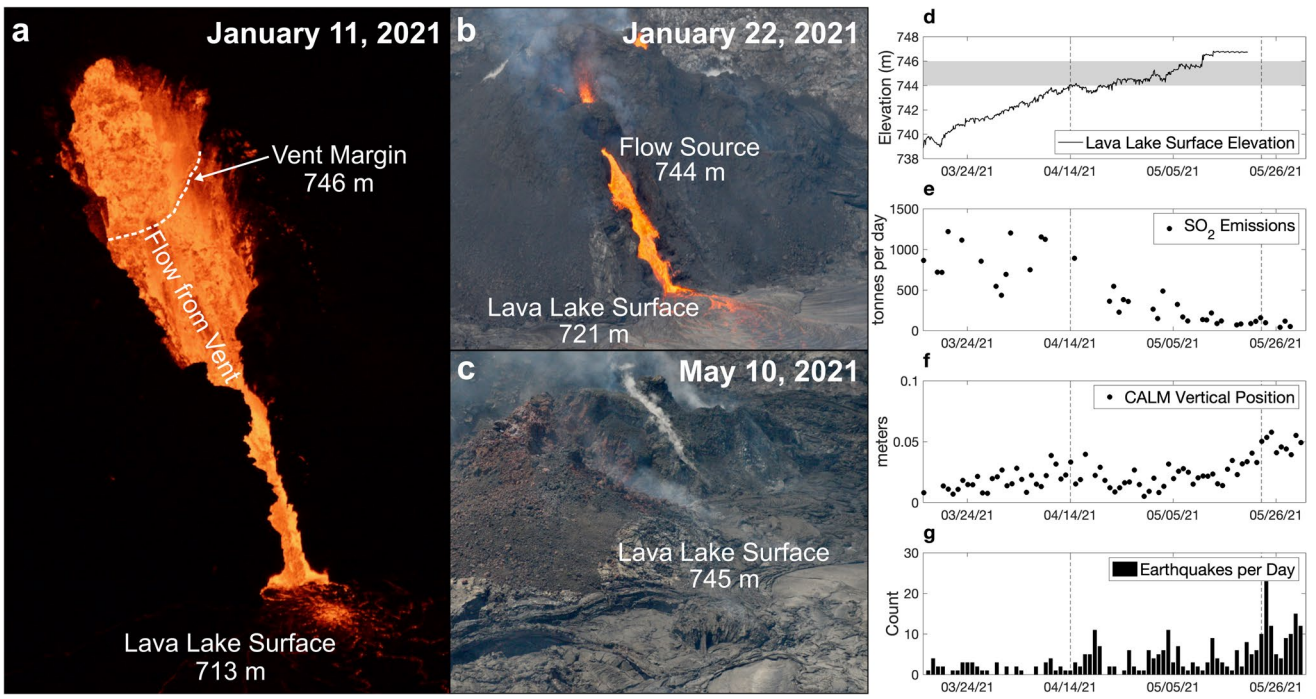

Fig. 8 In January, lava was observed flowing from the west vent at an elevation of 744–746 m (**a**–**b**). In May, the lake level was at the elevation of the observed flow in January (**c**, gray region in **d**). The lava lake reached 744 m on 14 April (left dashed vertical line, **d**–**g**). Emission of SO_2 decreased at this time (**e**) and the number of daily earthquakes recorded at the summit increased (**g**). In mid–late May, inflation of the volcano (**f**) and earthquake frequency (**g**) increased. The last mobile lava on the lake surface was observed on 23 May (right dashed vertical line, **d**–**g**)

suppressing vesiculation and increasing lava density) and initiate a month-long waning trend that resulted in the end of the 2020–2021 eruption in late May.

The end of an eruption can also be explained by a simple model of elastic strain relaxation in the crust surrounding a shallow storage region (Wadge 1981). Eruptions of this type have sharp onsets with effusion rate rapidly increasing to a maximum and then a waning phase with an exponential decline in effusion rate. During an eruption, if the maximum effusion rate and at least one other effusion rate during the waning phase are known, this pattern can be modeled to predict the duration of the eruption (Wadge et al., 1981; Bonny and Wright 2017). We apply this model of exponetial decay of effusion rate following the peak value (Eq. 7, Wadge et al., 1981; eqs. 1 and 2, Bonny and Wright 2017) to our data for the 2020–2021 eruption of Kīlauea. Our best-fit model agrees well with the decline in effusion rate through early January, suggesting that relaxation of strain built up during pre-eruption pressurization can explain the effusion rates during the first ~ 2 weeks of the eruption. However, this model underestimates the relatively steady TADR in February–April and predicts a much earlier end to the eruption than was observed. Additionally, deformation at the summit of Kīlauea does not show a steady deflationary trend as would be expected from a strain relaxation process. Instead, after a brief deflationary period between eruption onset and shutdown of the north vent, the summit slowly inflated until flattening out in April (Fig. 3e), suggesting a persistent driving force to the eruption during this period. The TADR during this steady period (~ 1–3 m^3 s^{-1}, bulk) was less than estimates for the background magma supply rate to Kīlauea (~ 3 m^3 s^{-1} DRE; Swanson 1972; Dvorak and Dzurisin 1993; Anderson and Poland 2016), so it is reasonable that the summit area could continue to inflate during an ongoing eruption. This, along with the relatively constant mobile lake surface area during the same period (Fig. 3c), suggests that pressure conditions in the shallow storage region beneath Halema‘uma‘u reached a steady state where a relatively low rate of lava supply to the surface could be sustained.

We conclude that the likely explanation for the mechanism causing the 2020–2021 eruption to end is vent drowning when the elevation of the lava lake surface surpassed the elevation of lava outflow from the vent. This follows conclusions from studies of previous passive lava lake and fissure eruptions that ended when ponded lava rose above the vent level (Wright et al. 1968; Richter et al. 1970; Peck and Kinoshita 1976; Wilson et al 1995; Jones et al. 2017). We cannot rule out the eruption ending due to internal magma chamber or plumbing processes, but monitoring data lack clear evidence for such a mechanism. Elastic strain relaxation was an essential process during the eruption, though it did not ultimately dictate the end of the eruption. Pressure that built up in the 2 years prior to the eruption (since the 2018 eruption ended) had to be released so that ascent could decline to a rate low enough where the lava overburden at the vent could suppress continued effusion. Our conclusion further demonstrates that detailed monitoring of TADR, crater geometry, and lava lake elevation provide a means to anticipate the end of an eruption by identifying when vent drowning may occur. Using the TADR and lake surface elevation from 16 February (Table 1) and projecting how long it would take to fill Halema‘uma‘u to an elevation of 745 m yields a result of 63 days, or 19 April, which is within a few days of when the eruption began to wane. Using the values from 16 April (Table 1), yields a forcast end date of 13 May, which is within a few days of when the eruption ended.

Conclusions

The 20 December 2020 eruption within Halema‘uma‘u crater at Kīlauea volcano ended a 27-month period of inactivity following the 2018 LERZ eruption. We used images collected on helicopter overflights and SfM photogrammetry to create a dense record of the growth of a passive lava lake in Halema‘uma‘u during the 5-month-long eruption. Effusion rates initially exceeded 100 m^3 s^{-1} but declined to < 10 m^3 s^{-1} about a week into the eruption and then stabilized at ~ 1 m^3 s^{-1} from February through April. This suggests initial effusion was controlled by relaxation of pressure built up due to magma accumulation in the Halema‘uma‘u shallow storage region prior to the eruption, before a relatively steady state was reached at effusion rates equal to or less than the background magma supply rate to Kīlauea. The lava lake consisted of two surface types, a mobile surface with horizontal flow of lava away from the vent and an immobile surface with a solid, stable crust. The mobile surface was perched a few meters above the immobile surface and was contained within levees. This surface was likely a thin layer (a few meters) of relatively low-density, vesicular lava recently erupted from the vent with a sharp boundary between the denser, degassed, and stagnant lava below. The addition of lava to the lake was accomodated beneath the immobile surface crust and the lake grew endogenously through vertical uplift of the crust. The area of the mobile lake surface was a proxy for the TADR, as the area declined rapidly in the first month of the eruption and then stabilized in February–April. Multiple types of monitoring data tracking the eruption showed a 3–4 week decline in activity from mid-April through mid-May. The eruption ended when the lava lake surface exceeded the elevation of lava outflow from the west vent and drowned the vent. The eruption filled Halema‘uma‘u with $40.6 \pm 0.5 \times 10^6$ m^3 of lava and the lava lake reached a maximum depth of 225 m.

Acknowledgements The entire staff of the Hawaiian Volcano Observatory (HVO) assisted in the collection and interpretation of field observations, installation and maintenance of monitoring equipment, and support of this work. Hawai'i Volcanoes National Park supported HVO staff access to closed areas of the park for eruption monitoring purposes. This work was supported by the Additional Supplemental Appropriations for Disaster Relief Act of 2019 (P.L. 116-20). Any use of trade, firm, or product names is for descriptive purposes only and does not imply endorsement by the U.S. Government.

Author contributions Conceptualization: Brett B. Carr, Matthew R. Patrick, Hannah R. Dietterich, Carolyn E. Parcheta; Methodology: Brett B. Carr, Matthew R. Patrick, Hannah R. Dietterich, Carolyn E. Parcheta, Michael H. Zoeller, Patricia A. Nadeau; Formal analysis and investigation: Brett B. Carr; Funding acquisition: Brett B. Carr, Matthew R. Patrick, Hannah R. Dietterich, Carolyn E. Parcheta, Christopher W. Hamilton; The first draft of the manuscript was written by Brett B. Carr and all authors commented on previous versions of the manuscript. All authors read and approved the final manuscript.

Funding Funding for author BBC while at the Hawaiian Volcano Observatory was provided by the U.S. Geological Survey Mendenhall Postdoctoral Fellowship program, position 17–16. BBC and CWH also acknowledge support from NASA's PSTAR program (Grant # 80NSSC21K0011).

Data availability The orthomosaics, DEMs, and GIS shapefiles generated for this study are openly available through a data release from the U.S. Geological Survey at https://doi.org/10.5066/P1IHM3GT.

Declarations

Conflicts of interest The authors have no competing interests to declare that are relevant to the content of this article.

References

Anderson KR, Poland MP (2016) Bayesian estimation of magma supply, storage, and eruption rates using a multiphysical volcano model: Kīlauea Volcano, 2000–2012. Earth Planet Sci Lett. https://doi.org/10.1016/j.epsl.2016.04.029

Anderson KR, Johanson IA, Patrick MR, Gu M, Segall P, Poland MP, Montgomery-Brown EK, Miklius A (2019) Magma reservoir failure and the onset of caldera collapse at Kīlauea Volcano in 2018. Science. https://doi.org/10.1126/science.aaz1822

Bonny E, Wright R (2017) Predicting the end of lava flow-forming eruptions from space. Bull Volcanol. https://doi.org/10.1007/s00445-017-1134-8

Bruce PM, Huppert HE (1989) Thermal control of basaltic fissure eruptions. Nature. https://doi.org/10.1038/342665a0

Burgi P-Y, Darrah TH, Tedesco D, Eymold WK (2014) Dynamics of the Mount Nyiragongo lava lake. J Geophys Res Solid Earth. https://doi.org/10.1002/2013jb010895

Cahalan RC, Mastin LG, Van Eaton AR, Hurwitz S, Smith AB, Dufek J, Solovitz SA, Patrick M, Schmith J, Parcheta C, Thelen WA, Downs DT (2023) Dynamics of the December 2020 ash-poor plume formed by lava-water interaction at the summit of Kīlauea Volcano, Hawai'i. Geochem Geophys Geosyst. https://doi.org/10.1029/2022GC010718

Carbone D, Poland MP, Patrick MR, Orr TR (2013) Continuous gravity measurements reveal a low-density lava lake at Kīlauea Volcano, Hawai'i. Earth Planet Sci Lett. https://doi.org/10.1016/j.epsl.2013.06.024

Carr BB, Lev E, Sawi T, Bennett KA, Edwards CS, Soule SA, Vargas SV, Marliyani GI (2021) Mapping and classification of volcanic deposits using multi-sensor unoccupied aerial systems. Remote Sens Environ. https://doi.org/10.1016/j.rse.2021.112581

Carr BB, Zoeller MH, DeSmither LG, Downs DT, Hamilton CW, Mulliken K, Parcheta CE, Patrick MR (2025) Digital elevation models, orthomosaics, and GIS shapefiles of the 2020–2021 summit eruption at Kīlauea volcano, Island of Hawai'i: U.S. geological survey data release. https://doi.org/10.5066/P1IHM3GT

Dietterich HR, Diefenbach AK, Soule SA, Zoeller MH, Patrick MP, Major JJ, Lundgren PR (2021) Lava effusion rate evolution and erupted volume during the 2018 Kīlauea lower East Rift Zone eruption. Bull Volcanol. https://doi.org/10.1007/s00445-021-01443-6

Dvorak JJ, Dzurisin D (1993) Variations in magma supply rate at Kilauea Volcano, Hawaii. J Geophys Res Solid Earth. https://doi.org/10.1029/93jb02765

Greenland LP, Okamura AT, Stokes JB (1988) Constraints on the mechanics of the eruption. In: Wolfe EW (ed) The Pu'u 'Ō'ō eruption of Kilauea Volcano, Hawaii; episodes 1 through 20, January 3, 1983, through June 8, 1984, U.S. Geological Survey Professional Paper 1463, pp 155–174

Harris AJL (2009) The pit-craters and pit-crater-filling lavas of Masaya volcano. Bull Volcanol. https://doi.org/10.1007/s00445-008-0241-y

Helz RT (1980) Crystallization history of Kilauea Iki lava lake as seen in drill core recovered in 1967–1979. Bull Volcanol. https://doi.org/10.1007/bf02600365

Helz RT, Thornber CR (1987) Geothermometry of Kilauea Iki lava lake, Hawaii. Bull Volcanol 49(5):651–668. https://doi.org/10.1007/bf01080357

Hulme G, Fielder G (1977) Effusion rates and rheology of lunar lavas. Philosophical Transactions of the Royal Society of London. Series A, Mathematical and Physical Sciences. https://doi.org/10.1098/rsta.1977.0059

Jaggar TA (1947) Origin and development of craters. Geol Soc Am Mem 21. Waverly Press, Baltimore

James MR, Robson S (2012) Straightforward reconstruction of 3D surfaces and topography with a camera: accuracy and geoscience application. J Geophys Res Earth Surf. https://doi.org/10.1029/2011JF002289

James MR, Robson S, Smith MW (2017) 3-D uncertainty-based topographic change detection with structure-from-motion photogrammetry: precision maps for ground control and directly georeferenced surveys. Earth Surf Process Landf. https://doi.org/10.1002/esp.4125

James MR, Antoniazza G, Robson S, Lane SN (2020) Mitigating systematic error in topographic models for geomorphic change detection: accuracy, precision and considerations beyond off-nadir imagery. Earth Surf Process Landf. https://doi.org/10.1002/esp.4878

Johnson GR (1979) Porosity and Density of Kilauea Volcano Basalts, Hawaii. U.S. Geol Survey Prof Paper 1123-B, pp 1–6, https://doi.org/10.3133/pp1123AD

Jones TJ, Llewellin EW, Houghton BF, Brown RJ, Vye-Brown C (2017) Proximal lava drainage controls on basaltic fissure eruption dynamics. Bull Volcanol. https://doi.org/10.1007/s00445-017-1164-2

Lague D, Brodu N, Leroux J (2013) Accurate 3D comparison of complex topography with terrestrial laser scanner: Application to the Rangitikei canyon (N-Z). ISPRS J Photogramm Remote Sens. https://doi.org/10.1016/j.isprsjprs.2013.04.009

Lev E, Ruprecht P, Oppenheimer C, Peters N, Patrick M, Hernández PA, Spampinato L, Marlow J (2019) A global synthesis of lava lake dynamics. J Volcanol Geotherm Res. https://doi.org/10.1016/j.jvolgeores.2019.04.010

LeWinter AL, Anderson SW, Finnegan DC, Patrick MR, Orr TR (2021) Crater growth and lava-lake dynamics revealed through multitemporal terrestrial lidar scanning at Kīlauea Volcano, Hawai'i. In: Patrick M, Orr TR, Swanson D, Houghton B (eds) The 2008–2018 summit lava lake at Kīlauea Volcano, Hawai'i: U.S. Geological Survey Professional Paper 1867, p 26. https://doi.org/10.3133/pp1867C

Mangan MT, Helz RT (1986) The distribution of vesicles and olivine phenocrysts in samples from drill hole KI 79–3, Kilauea Iki lava lake, Hawaii, Open-File Report. US Geological Survey. https://doi.org/10.3133/ofr86424

Moore JG (2001) Density of basalt core from Hilo drill hole. Hawaii J Volcanol Geotherm Res 112:221–230. https://doi.org/10.1016/s0377-0273(01)00242-6

Mosbrucker AR, Zoeller MH, Ramsey DW (2020) Digital elevation model of Kīlauea Volcano, Hawai'i, based on July 2019 airborne lidar surveys: U.S. Geological Survey data release. https://doi.org/10.5066/P9F1ZU8O

Nadeau, PA, Kern C, Cappos MJ, Elias T, Warren SM, Lerner AH, Sealing CR, Slagle CL, Moisseeva N, Holland LD, Clor L, Werner CA (2023) Sulfur dioxide emission rates from Hawaiian volcanoes, 2018–2022: U.S. Geological Survey data release. https://doi.org/10.5066/P9SNW2B7

Nadeau PA, Hurwitz S, Peek S, Lerner AH, Younger EF, Patrick MR, Damby DE, McCleskey RB, Kelly PJ (2024) Chemistry, growth, and fate of the unique, short-lived (2019–2020) water lake at the summit of Kīlauea Volcano, Hawaii. Geochem Geophys Geosyst 25(3):e2023GC011154. https://doi.org/10.1029/2023GC011154

National Academies of Sciences Engineering, Medicine (2017) Volcanic eruptions and their repose, unrest, precursors, and timing. The National Academies Press, Washington, DC. https://doi.org/10.17226/24650

Neal CA, Brantley SR, Antolik L, Babb JL, Burgress M, Calles K, Cappos M, Chang JC, Conway S, Desmither L, Dotray P, Elias T, Fukunaga P, Fuke S, Johanson IA, Kamibayahsi K, Kauahikaua J, Lee RL, Pekalib S, Mikilius A, Million W, Moniz CJ, Nadeau PA, Okubo P, Parcheta C, Patrick MR, Shiro B, Swanson DA, Tollett W, Trusdell F, Younger EF, Zoeller MH, Montgomery-Brown EK, Anderson KR, Poland MP, Ball JL, Bard J, Coombs M, Dietterich HR, Kern C, Thelen WA, Cervelli PF, Orr T, Houghton BF, Gansecki C, Hazlett R, Lundgren P, Diefenbach AK, Lerner AH, Waite G, Kelly P, Clor L, Werner C, Mulliken K, Fisher G, Damby D (2019) The 2018 rift eruption and summit collapse of Kīlauea Volcano. Science. https://doi.org/10.1126/science.aav7046

Oppenheimer C, Yirgu G (2002) Thermal imaging of an active lava lake: Erta Ale volcano, Ethiopia. Int J Remote Sens. https://doi.org/10.1080/01431160110114637

Orr TR (2014) The June-July 2007 collapse and refilling of Pu'u 'Ō'ō Crater, KÏlauea Volcano, Hawai'i. U.S. Geological Survey Scientific Investigations Report 2014–5124, p 15. https://doi.org/10.3133/sir20145124

Orr TR, Poland MP, Patrick MR, Thelen WA, Sutton AJ, Elias T, Thornber CR, Parcheta C, Wooten KM (2015) Kīlauea's 5–9 March 2011 Kamoamoa Fissure Eruption and Its Relation to 30+ Years of Activity From Pu'u 'Ō'ō. In: Carey R, Cayol V, Poland M, Weis D (eds) Hawaiian Volcanoes: From Source to Surface, Geophys. Monogr. Wiley, Hoboken, NJ, pp 393–420. https://doi.org/10.1002/9781118872079.ch18

Orr TR, Llewellin EW, Patrick MR (2022) Development, structure, and behavior of a perched lava channel at Kilauea Volcano, Hawai'i, during 2007. J Volcanol Geotherm Res. https://doi.org/10.1016/j.jvolgeores.2022.107637

Over JR, Ritchie AC, Kranenburg CJ, Brown JA, Buscombe D, Noble T, Sherwood CR, Warrick JA, Wernette PA (2021) Processing coastal imagery with Agisoft Metashape Professional Edition, version 1.6—Structure from motion workflow documentation: U.S. Geological Survey Open-File Report 2021–1039, 46 https://doi.org/10.3133/ofr20211039

Patrick MR, Orr TR (2012) Rootless shield and perched lava pond collapses at Kīlauea Volcano, Hawai'i. Bull. Volcanol. https://doi.org/10.1007/s00445-011-0505-9

Patrick MR, Orr TR (2018) Operational tracking of lava lake surface motion at Kīlauea Volcano, Hawai'i,: U.S. Geological Survey Techniques and Methods 13–A3, 12 p., https://doi.org/10.3133/tm13A3

Patrick MR, Orr T, Antolik L, Lee L, Kamibayashi K (2014) Continuous monitoring of Hawaiian volcanoes with thermal cameras. J Appl Volcanol. https://doi.org/10.1186/2191-5040-3-1

Patrick MR, Orr TR, Swanson DA, Lev E (2016) Shallow and deep controls on lava lake surface motion at Kīlauea Volcano. J Volcanol Geotherm Res. https://doi.org/10.1016/j.jvolgeores.2016.11.010

Patrick MR, Orr T, Fisher G, Trusdell F, Kauahikaua J (2017) Thermal mapping of a pāhoehoe lava flow, Kīlauea Volcano. J Volcanol Geotherm Res. https://doi.org/10.1016/j.jvolgeores.2016.12.007

Patrick MR, Orr TR, Swanson DA, Elias T, Shiro B (2018) Lava lake activity at the summit of Kīlauea Volcano in 2016: U.S. Geological Survey Scientific Investigations Report 2018–5008, 58 p., https://doi.org/10.3133/sir20185008

Patrick MR, Orr TR, Swanson D, Houghton B, Wooten K, Desmither L, Parcheta C, Fee D (2021) Kīlauea's 2008–2018 summit lava lake—Chronology and eruption insights. In Patrick MR, Orr T, Swanson D, Houghton B (eds) The 2008–2018 summit lava lake at Kīlauea Volcano, Hawai'i: U.S. Geological Survey Professional Paper 1867, p 50

Patrick MR, Younger EF, Tollett WD (2022) Thermal camera data for the summit of Kīlauea Volcano, 2019–2022: U.S. Geological Survey data release. https://doi.org/10.5066/P9HQHDMH

Patrick MR, Zoeller MH, Trusdell FA, Downs DT, Lynn KJ, Deligne NI, Mulliken K, Gallant E, Chang JM, Schmith J, Chang J, Dotray P, Johanson I, Nadeau P, Carr BB (2023) Patterns of crater-refilling eruptions at the summit of Kīlauea, 2020- present. Abstract V22B-02, AGU Fall Meeting, San Francisco, CA, 11-15 Dec

Patrick MR, Orr TR, Tollett WD, Kamibayashi KP (2024) Thermal camera images of lava lake and crater filling activity at Pu'u'ō'ō, East Rift Zone of Kīlauea Volcano, Island of Hawai'i, 2011-2019. U.S. Geological Survey data release. https://doi.org/10.5066/P9CYSYQJ

Peck DL (1978) Cooling and vesiculation of Alae lava lake, Hawaii, Professional Paper. US Geological Survey. https://doi.org/10.3133/pp935b

Peck DL, Kinoshita WT (1976) The eruption of August 1963 and the formation of Alae lava lake, Hawaii, Professional Paper. US Geological Survey. https://doi.org/10.3133/pp935a

Pedersen GBM, Belart JMC, Óskarsson BV, Gudmundsson MT, Gies N, Högnadóttir T, Hjartardóttir ÁR, Pinel V, Berthier E, Dürig T, Reynolds HI, Hamilton CW, Valsson G, Einarsson P, Ben-Yehosua D, Gunnarsson A, Oddsson B (2022) Volume, effusion rate, and lava transport during the 2021 Fagradalsfjall eruption: results from near real-time photogrammetric monitoring. Geophys Res Lett. https://doi.org/10.1029/2021gl097125

Perret FA (1913) The floating islands of Halemaumau. Am J Sci 4(207):273–282

Poland MP, Dalfsen EZ-V, Bagnardi M, Johanson IA (2019) Post-Collapse Gravity Increase at the Summit of Kīlauea Volcano, Hawai'i. Geophys Res Lett. https://doi.org/10.1029/2019gl084901

Richter DH, Eaton JP, Murata KJ, Ault WU, Krivoy HL (1970) Chronological narrative of the 1959–60 eruption of Kilauea Volcano, Hawaii. Professional Paper. US Geological Survey. https://doi.org/10.3133/pp537e

Shiro BR, Zoeller MH, Kamibayashi K, Johanson IA, Parcheta C, Patrick MR, Nadeau P, Lee L, Miklius A (2020) Monitoring network

changes during the 2018 Kīlauea volcano eruption. Seismol Res Lett. https://doi.org/10.1785/0220200284

Snavely N, Seitz SM, Szeliski R (2008) Modeling the world from internet photo collections. Int J Comput Vis. https://doi.org/10.1007/s11263-007-0107-3

Sparks RSJ (1978) The dynamics of bubble formation and growth in magmas: a review and analysis. J Volcanol Geotherm Res. https://doi.org/10.1016/0377-0273(78)90002-1

Stovall WK, Houghton BF, Harris AJL, Swanson DA (2009) Features of lava lake filling and draining and their implications for eruption dynamics. Bull Volcanol. https://doi.org/10.1007/s00445-009-0263-0

Stovall WK, Houghton BF, Harris AJL, Swanson DA (2009) A frozen record of density-driven crustal overturn in lava lakes: the example of Kīlauea Iki 1959. Bull Volcanol. https://doi.org/10.1007/s00445-008-0225-y

Sutton AJ, Elias T, Kauahikaua J (2003) Lava-Effusion Rates for the Pu‘u ‘Ō‘ō-Kūpaianaha Eruption Derived from SO_2 Emissions and Very Low Frequency (VLF) Measurements. In: Heliker, C.C., Swanson, D.A., Takahashi, T.J. (Eds.) The Pu‘u ‘Ō‘ō-Kūpaianaha eruption of Kīlauea Volcano, Hawai‘i: The first 20 years, US Geological Survey Professional Paper 1676, pp. 137–148. https://doi.org/10.3133/pp1676

Swanson DA (1972) Magma supply rate at Kilauea Volcano, 1952–1971. Science. https://doi.org/10.1126/science.175.4018.169

Swanson DA, Duffield WA, Jackson DB, Peterson DW (1972) The complex filling of alae crater, Kilauea Volcano, Hawaii. Bull. Volcanol. https://doi.org/10.1007/bf02596984

Swanson DA, Duffield WA, Jackson DB, Peterson DW (1979) Chronological narrative of the 1969–71 Mauna Ulu eruption of Kilauea Volcano, Hawaii. Professional Paper. US Geological Survey. https://doi.org/10.3133/pp1056

Thielicke W, Sonntag R (2021) Particle image velocimetry for MATLAB: accuracy and enhanced algorithms in PIVlab. J Open Res Softw. https://doi.org/10.5334/jors.334

Tilling RI (1987) Fluctuations in surface height of active lava lakes during 1972–1974 Mauna Ulu Eruption, Kilauea Volcano, Hawaii. J. Geophys. Res. Solid Earth https://doi.org/10.1029/jb092ib13p13721

Wadge G (1981) The variation of magma discharge during basaltic eruptions. J Volcanol Geotherm Res. https://doi.org/10.1016/0377-0273(81)90020-2

Walker GPL (1993) Basaltic-volcano systems. Geological Society, London, Special Publications 76:3–38. https://doi.org/10.1144/gsl.sp.1993.076.01.01

Westoby MJ, Brasington J, Glasser NF, Hambrey MJ, Reynolds JM (2012) ‘Structure-from-Motion’ photogrammetry: A low-cost, effective tool for geoscience applications. Geomorphology. https://doi.org/10.1016/j.geomorph.2012.08.021

Wilson L, Parfitt EA (1993) The formation of perched lava ponds on basaltic volcanoes: the influence of flow geometry on cooling-limited lava flow lengths. J Volcanol Geotherm Res. https://doi.org/10.1016/0377-0273(93)90053-t

Wilson L, Parfitt EA, Head JW (1995) Explosive volcanic eruptions-VIII. The role of magma recycling in controlling the behaviour of Hawaiian-style lava fountains. Geophys J Int. https://doi.org/10.1111/j.1365-246x.1995.tb03522.x

Wolfe EW, Neal CA, Banks NG, Duggan TJ (1988) Geologic observations and chronology of eruptive events. In: Wolfe EW (ed) The Pu‘u ‘Ō‘ō eruption of Kilauea Volcano, Hawaii; episodes 1 through 20, January 3, 1983, through June 8, 1984, U.S. Geological Survey Professional Paper 1463, pp. 1–97. https://doi.org/10.3133/pp1463

Wright TL, Okamura RT (1977) Cooling and Crystallization of tholeiitic basalt, 1965 Makaopuhi Lava Lake, Hawaii. In: US geological survey professional paper 1004. https://doi.org/10.3133/pp1004

Wright TL, Kinoshita WT, Peck DL (1968) March 1965 eruption of Kilauea volcano and the formation of Makaopuhi Lava Lake. J Geophys Res 73:3181–3205. https://doi.org/10.1029/jb073i010p03181

Wright TL, Peck DL, Shaw HR (1976) Kilauea Lava Lakes: Natural Laboratories for Study of Cooling, Crystallization, and Differentiation of Basaltic Magma. In: Sutton GH, Manghnani MH, Moberly R, Mcafee EU (eds) The Geophysics of the Pacific Ocean Basin and Its Margin, American Geophysical Union, pp 375–390. https://doi.org/10.1029/gm019p0375

Younger EF, Tollett W, Patrick MR (2024) Continuous laser rangefinder measurements of lava lake elevation and crater filling at the summit of Kīlauea volcano, Island of Hawai‘i, 2021–2024: U.S. Geological Survey data release. https://doi.org/10.5066/P13SQTIC

Younger EF, Tollett W, Patrick MR (2025) Monitoring lava lake fluctuations and crater refilling with continuous laser rangefinders. J Appl Volcanol. https://doi.org/10.1186/s13617-025-00152-5